Appendix

The AAA+ ATPase TRIP13 remodels HORMA domains through N-terminal engagement and unfolding

Qiaozhen Ye, Dong Hyun Kim, Ihsan Dereli, Scott C. Rosenberg, Goetz Hagemann, Franz Herzog, Attila Tóth, Don W. Cleveland, Kevin D. Corbett

Table of Contents

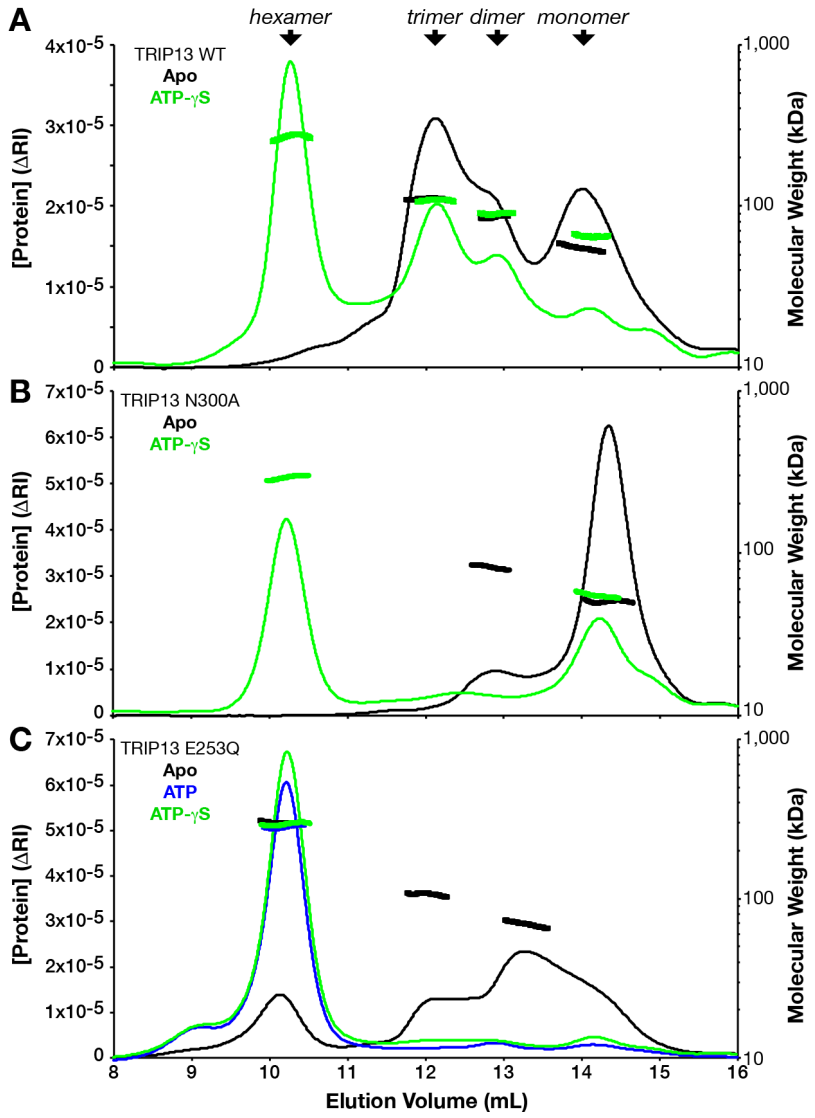

TRIP13 WT	Meas. MW	Calc. MW
Apo - Trimer	110 +/- 3.2 kDa	146 kDa
Apo - Dimer	81 +/- 2.3 kDa	97 kDa
Apo - Monomer	54 +/- 1.8 kDa	49 kDa
ATP-γS - Hexamer	270 +/- 7.8 kDa	291 kDa
ATP-γS - Trimer	109 +/- 2.8 kDa	146 kDa
ATP-γS - Dimer	86 +/- 2.1 kDa	97 kDa
ATP-γS - Monomer	65 +/- 2.2 kDa	49 kDa

TRIP13 N300A	Meas. MW	Calc. MW
Apo - Dimer	81 +/- 1.9 kDa	97 kDa
Apo - Monomer	50 +/- 1.8 kDa	49 kDa
ATP-γS - Hexamer	288 +/- 9.2 kDa	291 kDa
ATP-γS - Monomer	54 +/- 2.1 kDa	49 kDa

TRIP13 E253Q	Meas. MW	Calc. MW
Apo - Hexamer	297 +/- 8.9 kDa	291 kDa
Apo - Trimer	105 +/- 2.8 kDa	146 kDa
Apo - Dimer	68 +/- 2.0 kDa	97 kDa
ATP - Hexamer	285 +/- 9.4 kDa	291 kDa
ATP-γS - Hexamer	291 +/- 8.4 kDa	291 kDa

Appendix Figure S1 - Oligomeric state of TRIP13.

(A-C) Size exclusion chromatography/multi-angle light scattering (SEC-MALS) analysis of TRIP13 wild-type (A), N300A (B), and E253Q (C). Samples without added nucleotide are shown in black, with ATP-γS in green, and ATP (E253Q only) in blue. Thin lines indicate protein concentration (measured by change in refractive index, left axis), and thick lines indicate measured molecular weight (right axis). Best-fit TRIP13 oligomeric state for each peak, determined by measured molecular weights is shown above panel (A). For each construct, the measured and calculated molecular weights of each peak are shown in tables (right). For assembly of the TRIP13:p31^{comet}:MAD2 complex (**Fig 1B,C**), TRIP13^{E253Q} was pre-incubated with ATP.

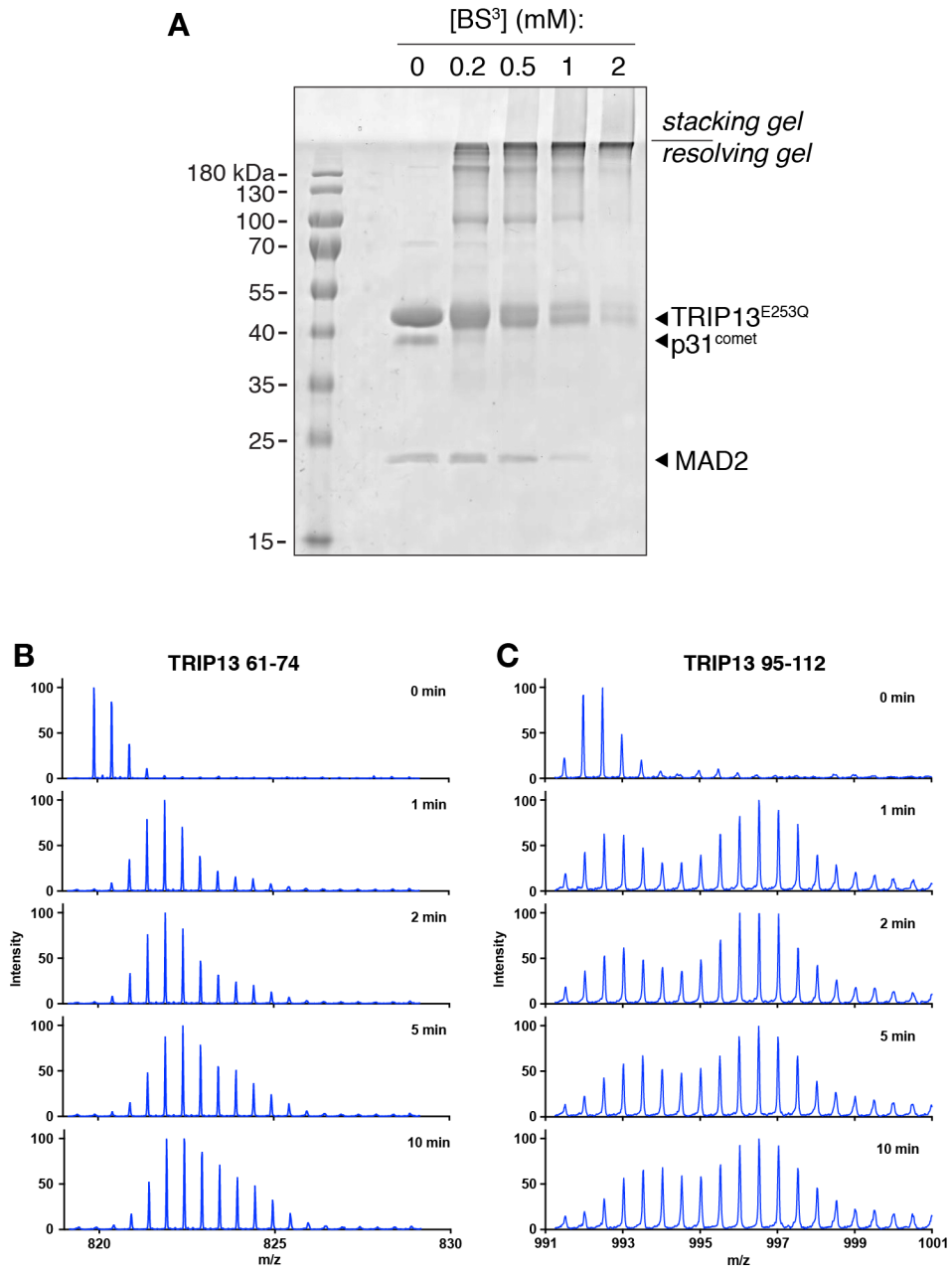

Appendix Figure S2 - TRIP13^{E253Q}:p31^{comet}:MAD2 XLMS and HDX-MS.

(A) Chemical crosslinking of TRIP13^{E253Q}:p31^{comet}:MAD2 with BS^3 at the indicated concentrations. Mass spectrometry was performed on all four crosslinked samples (see **Fig 2** and **Tables EV2, EV3**).
(B) Example mass spectra of the TRIP13 61-74 peptide (+2 charge state), in TRIP13^{E253Q} alone after 0, 1, 2, 5, and 10 minutes of H-D exchange. Early time-points show monoodal H-D exchange, while later time-points show limited bimodal exchange.
(C) Example mass spectra of a strongly bimodal peptide, TRIP13 residues 95-112 (+2 charge state), in TRIP13^{E253Q} alone after 0, 1, 2, 5, and 10 minutes of H-D exchange.

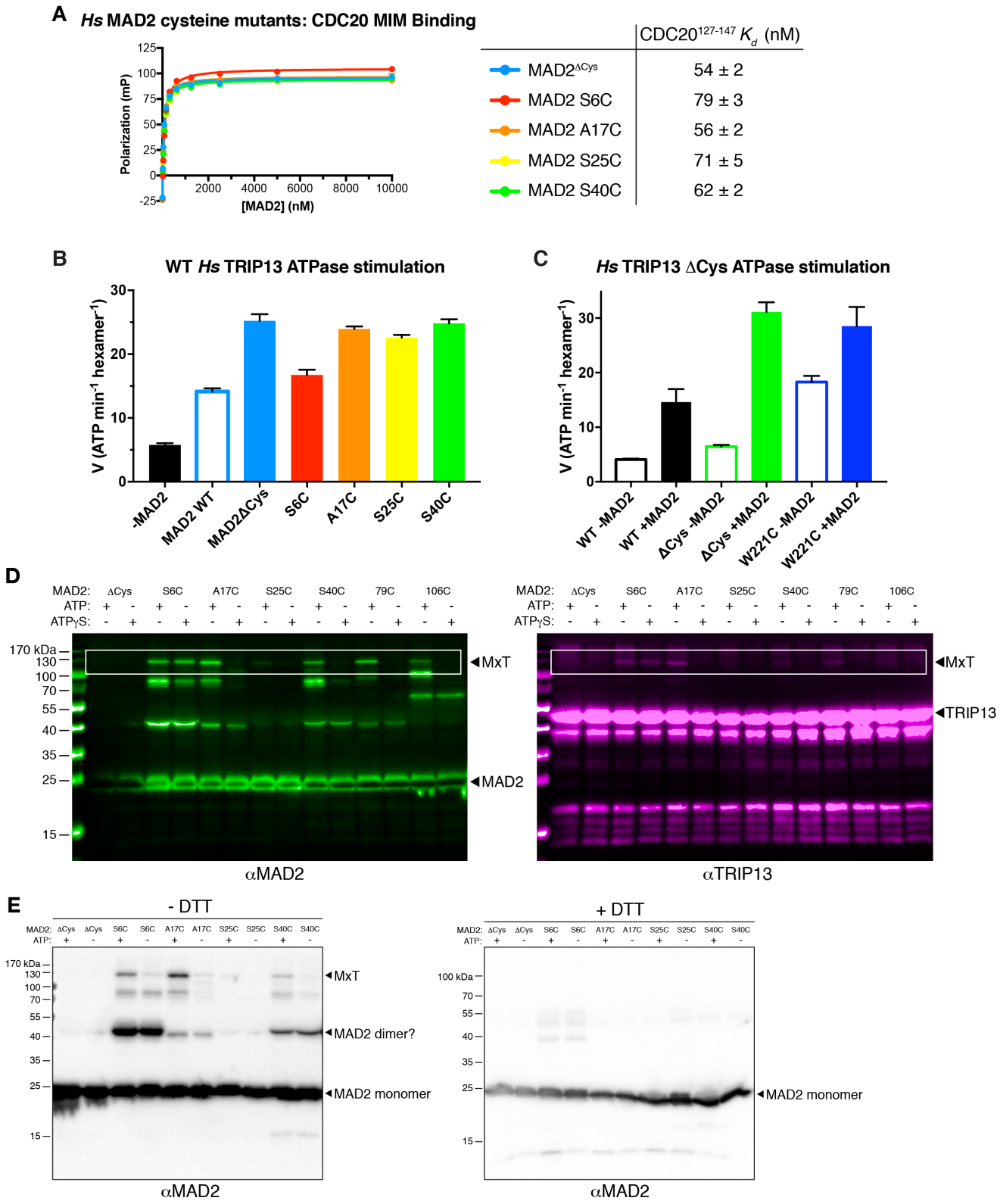

Appendix Figure S3 - MAD2/TRIP13 cysteine mutant validation and crosslinking.

(A) Fluorescence polarization assay showing binding of *H. sapiens* MAD2$^{\Delta Cys}$ and non-native cysteine mutants to the closure motif-containing CDC20$^{127\text{-}147}$ peptide.

(B) Stimulation of *H. sapiens* TRIP13 ATP hydrolysis by MAD2 wild-type, MAD2$^{\Delta Cys}$, and non-native cysteine mutants.
(C) ATP hydrolysis by TRIP13$^{\Delta Cys}$ and W221C.
(D) Full gels from **Fig 3C**, with boxed regions in that figure shown as white outlines. Positions of unreacted MAD2 and TRIP13, and the crosslinked MAD2-TRIP13 species (MxT) are shown. Additional bands detected by anti-MAD2 antibodies likely represent crosslinked MAD2 dimers or MAD2:p31^{comet} complexes.
(E) Non-reducing (left) versus reducing (right) SDS-PAGE analysis of selected crosslinking reactions, showing disappearance of the crosslinked species upon addition of reducing agent (DTT).

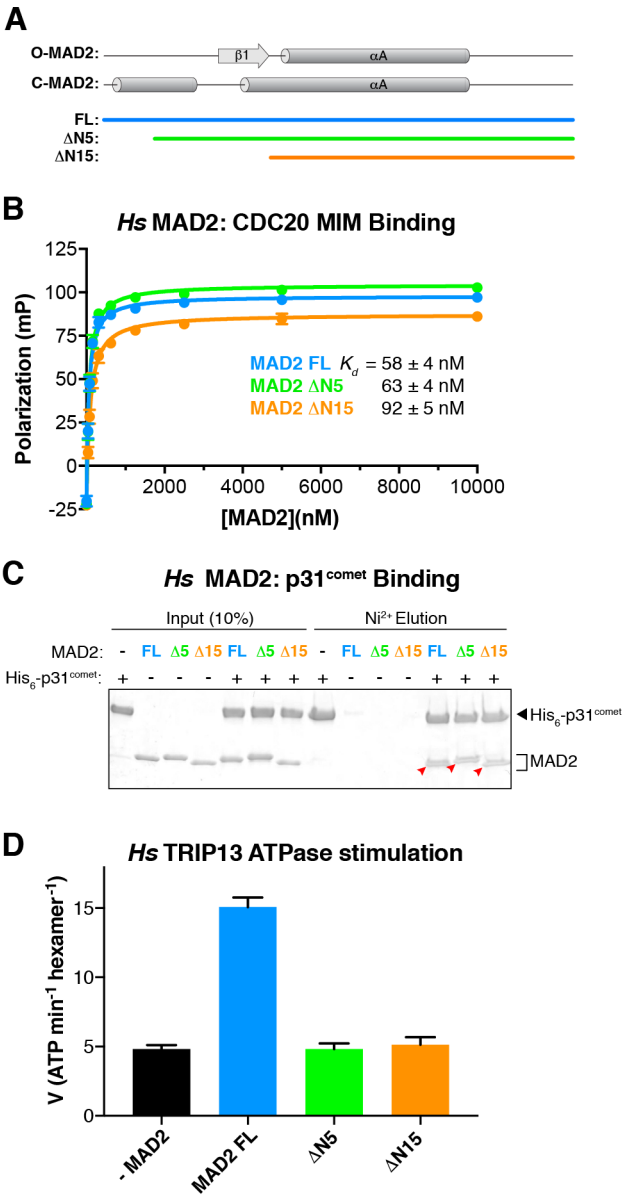

Appendix Figure S4 - Biochemical characterization of *H. sapiens* MAD2 ΔN mutants.

(A) Schematic of the MAD2 N-terminus, with secondary structure and the limits of FL, ΔN5, and ΔN15 constructs.

(B) Fluorescence polarization assay showing binding of *H. sapiens* MAD2 full-length (FL), ΔN5, and ΔN15 to the closure motif-containing CDC20$^{127\text{-}147}$ peptide (sequence identical in *M. musculus* and *H. sapiens* CDC20).

(C) Pulldown assay showing binding of *H. sapiens* MAD2 full-length (FL), ΔN5, and ΔN15 to p31^{comet} (red arrowheads).

(D) ATP hydrolysis by *H. sapiens* TRIP13 in the presence of p31^{comet} and MAD2 FL, ΔN5, or ΔN15 (all *H. sapiens* proteins; MAD2 constructs included the R133A mutation).

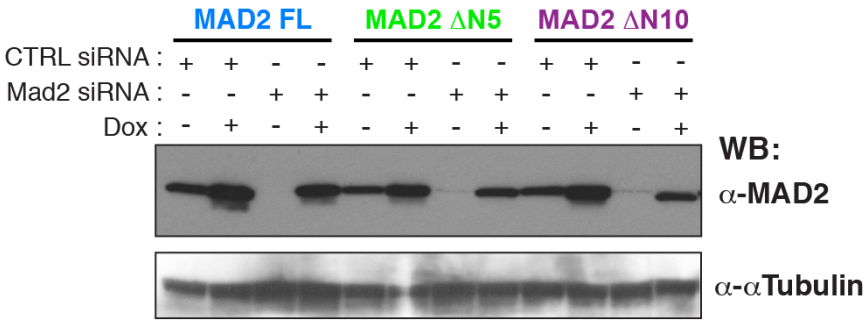

Appendix Figure S5 - Expression of MAD2 FL and ΔN mutants in DLD1 cells.

Western blot showing siRNA of endogenous MAD2 in DLD1 cells, and doxycycline (Dox)-induced expression of Flp-in MAD2 constructs (FL, ΔN5, and ΔN10).

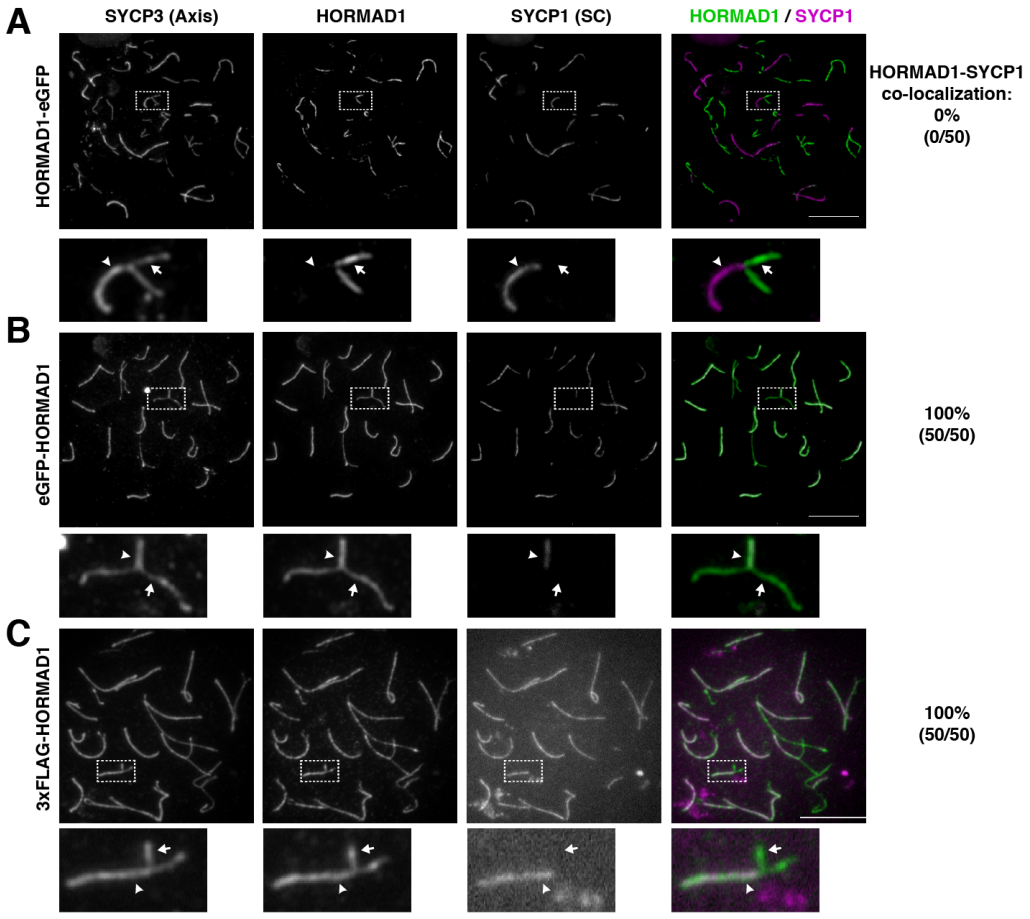

Appendix Figure S6 - N-terminal tags disrupt TRIP13-mediated removal of HORMAD1 from the meiotic chromosome axis.

(A-C) Chromosome localization of SYCP3 (chromosome axis), SYCP1 (synaptonemal complex/SC), and HORMAD1 in late zygotene/early pachytene mouse spermatocytes. While C-terminally tagged HORMAD1 (panel A; same as **Fig 6B**, shown here for comparison) is efficiently removed upon SC formation, N-terminal GFP (panel B) or FLAG (panel C) tags disrupt TRIP13-mediated removal.

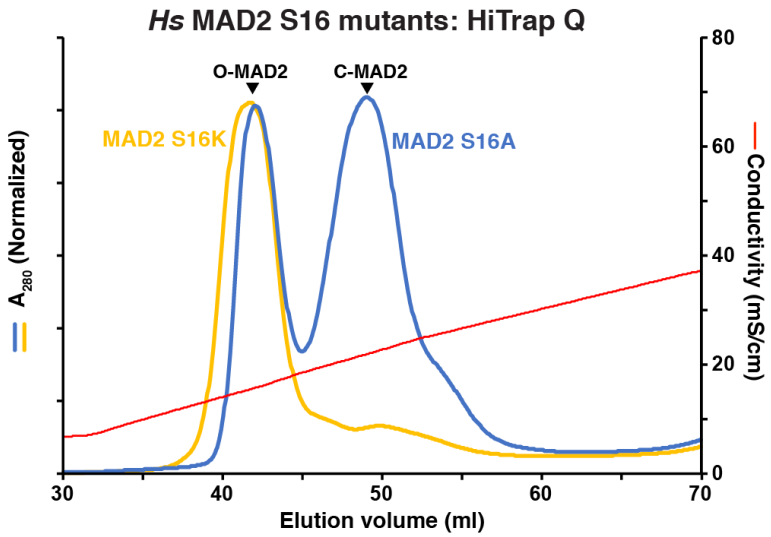

Appendix Figure S7 - Purification of MAD2 S16 mutants.

UV and conductivity traces from HiTrap Q HP purification of *H. sapiens* MAD2 S16A (blue) and S16K (yellow) mutants. For the experiments in **Fig 7C**, we pooled fractions containing O-MAD2 only. Similar analysis with C-MAD2^{S16A} fractions showed that this population is unstable, converting to O-MAD2 during subsequent gel-filtration and concentration steps, even though these steps were performed at 4°C (data not shown).

Material and Methods

Cloning and Protein Purification

Full-length human and mouse TRIP13, p31^{comet}, and MAD2 were amplified from cDNA clones and inserted into pET-based vectors with an N-terminal, TEV-protease cleavable His_6 tags, then variants were cloned using site-directed mutagenesis. For biochemical assays, full-length and N-terminally truncated mouse MAD2 constructs were cloned with an N-terminal His_6-SUMO tag, which can be cleaved with the SUMO isopeptidase Ulp1 to leave no non-native residues at the N-terminus of the recombinant protein (Malakhov *et al*, 2004; Butt *et al*, 2005). All MAD2 proteins used for biochemical assays contained the R133A mutant that compromised MAD2 homodimer formation (Sironi *et al*, 2001), which allows purification of separate O-MAD2 and C-MAD2 populations via ion-exchange chromatography. We originally designed three MAD2 N-terminal deletions removing 5, 10, and 15 residues, but the MAD2-ΔN10 mutant was not cleavable by Ulp1, so it was not used in *in vitro* assays. The coding sequence for TRIP13$^{\Delta Cys}$ (C14N, C93S, C264S, C341A; cysteines 189 and 334 were judged to be buried based on the TRIP13 crystal structure) was synthesized (GeneArt, Thermo-Fisher Scientific) and cloned as above, and MAD2$^{\Delta Cys}$ (C79S, C106S, C149A) was cloned by PCR-based mutagenesis. Additional cysteines (TRIP13 W221C; MAD2 S6C, A17C, S25C, and S40C, along with re-introduced C79 and C106) were introduced into TRIP13$^{\Delta Cys}$ and MAD2$^{\Delta Cys}$ by PCR-based mutagenesis.

Proteins were expressed in *E. coli* strain Rosetta2(DE3)pLysS (EMD Millipore) except for human TRIP13, which was expressed in *E. coli* LOBSTR (Kerafast, Inc.) (Andersen *et al*, 2013); expression was induced with IPTG for 16-20 hours at 20°C. Proteins were purified by Ni^{2+}-affinity (Ni-NTA; Qiagen) and ion-exchange (Hitrap SP HP or Hitrap Q HP; GE Healthcare) chromatography, His_6-tags were cleaved by incubation with TEV protease (Kapust *et al*, 2001) at 4°C overnight, and His_6-SUMO tags were cleaved by incubation with *S. cerevisiae* Ulp1 at 4°C overnight. Uncleaved protein, cleaved tags, and proteases were removed by passing cleavage reactions over a Ni^{2+}-affinity column a second time, and flow-through fractions were further purified by gel filtration (Superdex 200; GE Healthcare). For MAD2 R133A mutant proteins, O-MAD2 and C-MAD2 were separated on a HiTrap Q HP column (GE Healthcare), then separately purified thereafter and kept at 4°C to maintain conformation. Proteins were concentrated and stored at 4°C for crystallization, or at -80°C for biochemical assays.

Crystallization and Structure Determination

For crystallization, TRIP13^{E253Q} was concentrated to 15 mg/mL and exchanged into a buffer containing 25 mM Tris-HCl pH 7.5, 0.2 M NaCl, 5 mM $MgCl_2$, and 1 mM TCEP. For crystallization without ATP, TRIP13^{E253Q} was mixed 1:1 in hanging drop format with well solution containing 0.1 M Tris-HCl pH 8.5, 0.8 M LiCl, and 4% PEG 3350. Crystals (~90 x 90 x 50 μM) were cryoprotected by addition of 20% glycerol and flash-frozen in liquid nitrogen. For ATP-bound TRIP13^{E253Q}, 1 mM ATP was added to the protein solution, then protein was mixed 1:1 in hanging drop format with well solution containing 0.1 M Tris-HCl pH 8.5, 0.2 M KCl, 10% pentaerythritol propoxylate. Crystals (~100 x 100 x 60 μm) were cryoprotected by addition of 10% glycerol and 12% pentaerythritol propoxylate (22% total) and flash-frozen in liquid nitrogen.

Our initial crystallization trials were performed with TRIP13^{E253Q} in complex with p31^{comet} and MAD2 (purified as in the next section), but these proteins are not detected in final electron density maps and are

not essential for TRIP13 crystallization. We speculate that formation of the TRIP13 helical filament destroys a major element of the TRIP13-substrate interface (i.e. the top face of the TRIP13 hexamer), thereby destabilizing $p31^{comet}$:MAD2 binding. $TRIP13^{E253Q}$ crystals used for final data collection were grown in the absence of $p31^{comet}$ and MAD2.

X-ray diffraction datasets $TRIP13^{E253Q}$ apo and $TRIP13^{E253Q}$·ATP were collected on NE-CAT beamline 24ID-E at the Advanced Photon Source (Argonne National Laboratory, Argonne IL; see below for support statement). Crystals contained one monomer of TRIP13 per asymmetric unit. Data was processed by the in-house RAPD data-processing pipeline, incorporating XDS (Kabsch, 2010) for data reduction and AIMLESS (Evans & Murshudov, 2013) for scaling. Resolution cutoffs were determined using a $CC_{1/2}$ value (Pearson correlation coefficient of half-datasets) of ~0.5 (Karplus & Diederichs, 2012). Phasing was performed by molecular replacement with PHASER (McCoy *et al*, 2007), using a structure of *C. elegans* PCH-2 (PDB ID 4XGU) (Ye *et al*, 2015) with most side-chains removed. Initial models were iteratively rebuilt in COOT (Emsley *et al*, 2010) and refined using phenix.refine (Adams *et al*, 2010) with a consistent free-*R* set across multiple structures (**Table EV1**).

$TRIP13^{E253Q}$:$p31^{comet}$:MAD2 complex assembly and crosslinking mass spectrometry

For assembly of the $TRIP13^{E253Q}$:$p31^{comet}$:MAD2 complex, proteins were mixed in a final molar ratio of 2:1:1 (three copies of $p31^{comet}$:MAD2 per $TRIP13^{E253Q}$ hexamer) in a buffer containing 20 mM HEPES pH 7.5, 0.3 M NaCl, 5 mM $MgCl_2$, 5% glycerol and 1 mM ATP, then incubated for 60 minutes at 4°C. Complexes were injected onto a Superdex 200 Increase size exclusion column (GE Life Sciences) and fractions representing the $TRIP13^{E253Q}$ hexamer plus associated $p31^{comet}$ and MAD2 were pooled and concentrated to 1 mg/mL. Crosslinking was performed by addition of 0.2, 0.5, 1, or 2 mM isotopically-coded D_0/D_{12} BS^3 (bis-sulfosuccinimidylsuberate; Creative Molecules) for 30 minutes at 30°C. The reaction was quenched by the addition of 100 mM NH_4HCO_3. Quenched reactions were supplemented with 8M urea to a final concentration of 6M. Subsequent to reduction and alkylation, crosslinked proteins were digested with Lys-C (1:50 w/w, Wako) for 3 h, diluted with 50 mM ammonium bicarbonate to 1M urea and digested with trypsin (1:50 w/w, Promega) overnight. Crosslinked peptides were purified by reversed phase chromatography using C18 cartridges (Sep-Pak, Waters). Crosslink fractions by peptide size exclusion chromatography and analyzed by tandem mass spectrometry (Orbitrap Elite, Thermo Scientific) (Herzog *et al*, 2012). Fragment ion spectra were searched and crosslinks identified by the dedicated software program xQuest (Walzthoeni *et al*, 2015; Rinner *et al*, 2008).

Hydrogen-Deuterium Exchange Mass Spectrometry

HD exchange experiments were conducted with a Waters Synapt G2S system. We examined six samples (all *H. sapiens* proteins): (1) $MAD2^{R133A}$ in complex with a peptide encompassing residues 127-147 of CDC20 to maintain the C-MAD2 conformation; (2) $p31^{comet}$; (3) $TRIP13^{E253Q}$:ATP; (4) $MAD2^{R133A}$:$CDC20^{127-147}$ + $p31^{comet}$ (pre-mixed and purified by size exclusion chromatography) (5) $TRIP13^{E253Q}$:ATP + $p31^{comet}$ (purified by size-exclusion chromatography); and (6) $TRIP13^{E253Q}$:ATP + $MAD2^{R133A}$:$CDC20^{127-147}$ +$p31^{comet}$ (purified by size-exclusion chromatography). 5 uL samples containing 10 μM individual proteins or complexes in exchange buffer (300 mM NaCl, 20 mM Tris pH 7.5, 10% glycerol, 1 mM DTT) were mixed with 55 μL of the same buffer made with D_2O for several deuteration times (0 sec, 1 min, 2 min, 5 min, 10 min) at 15°C. The exchange was quenched for 2 min at 1°C with an equal volume of quench buffer (3M guanidine HCl, 0.1% formic acid). A portion of the quenched sample

(50 µL) was injected onto an online pepsin column (Applied Biosystems, Poroszyme Immobilized Pepsin cartridge). The resulting peptic peptides were then separated on a C18 column (Waters, Acquity UPLC BEH C18, 1.7 µm, 1.0 mm × 50 mm) fit with a Vanguard trap column using a 3-85% acetonitrile (containing 0.1% formic acid) gradient over 12 min at a flow rate of 40 µL/min. The separated peptides were directed into a Waters SYNAPT G2s quadrupole time-of-flight (qTOF) mass spectrometer. The mass spectrometer was set to collect data in the MSE, ESI+ mode; in a mass acquisition range of m/z 255.00−1950.00; with a scan time of 0.4 s. Continuous lock mass correction was accomplished with infusion of the LeuEnk peptide every 30 s (mass accuracy of 1 ppm for the calibration standard). The peptides were identified using PLGS version 2.5 (Waters, Inc.). The relative deuterium uptake for each peptide was calculated by comparing the centroids of the mass envelopes of the deuterated samples with the undeuterated controls using DynamX version 2.0 (Waters Corp.).

ATPase assays

ATPase reactions contained assay buffer (25 mM Tris-HCl at pH 7.5, 200 mM NaCl, 10 mM $MgCl_2$, 1 mM DTT, 5% glycerol) plus 250 µM ATP, and were incubated 30 minutes at 37°C. Reactions were stopped and triplicate samples were assayed using the ADP-Glo kinase assay kit (Promega) in 384-well microplates using a TECAN (Mannedorf, Switzerland) Infinite M1000 spectrophotometer. Most assays were performed with 100 or 200 nM TRIP13 (monomer concentration); below this concentration ATPase activity was highly inconsistent, potentially due of dissociation of the TRIP13 hexamer. For most assays, $p31^{comet}$ and MAD2 were added in excess, at 2 µM and 5 µM, respectively. Data were converted to K_{cat} using a standard curve for ADP, and fit using PRISM version 7 (GraphPad Software, La Jolla CA).

Protein interaction assays

For MAD2-$p31^{comet}$ binding assays, 10 µg His_6-$p31^{comet}$ was incubated with equimolar amounts of untagged MAD2 (FL or truncation mutants) in 50 µL binding buffer (20 mM HEPES pH 7.5, 200 mM NaCl, 5mM $MgCl_2$, 5% glycerol, 20mM imidazole, 1mM 2-ME, 0.1% NP-40), incubated 60 minutes at 20°C, then 30 µL of a 50% slurry of Ni-NTA resin (Qiagen) was added and the mixture incubated with agitation for a further 30 minutes. Beads were then washed with 3 x 0.5 mL binding buffer, then eluted with 25 µL elution buffer. Input and Ni-NTA bound samples were analyzed by SDS-PAGE.

For fluorescence polarization assays, N-terminal FITC-labeled CDC20 closure motif peptide (residues 127-147; EAKILRLSGKPQNAPEGYQNR) was synthesized (Biomatik) and resuspended in binding buffer (25 mM Tris-HCl pH 7.5, 200 mM NaCl, 5% glycerol, 1 mM DTT, 0.1% NP-40). Fifty µL reactions containing 10 nM peptide plus 40 nM-40 µM MAD2 (FL or N-terminal truncations) were incubated 30 minutes at room temperature, then fluorescence polarization was read in 384-well plates using a TECAN Infinite M1000 PRO fluorescence plate reader. All binding curves were done in triplicate. Binding data were analyzed with Graphpad Prism v. 7 using a single-site binding model.

Cysteine crosslinking

Cysteine crosslinking assays were performed essentially as described (Yang *et al*, 2015). Cysteine-activated MAD2 was prepared by: (1) incubating in crosslinking buffer (50 mM HEPES pH 7.5, 200 mM NaCl, 5 mM $MgCl_2$, 5% glycerol) + 5 mM DTT for 60 minutes at 20°C; (2) buffer-exchange into DTT-free crosslinking buffer (Zeba-Spin desalting columns, Thermo Scientific) followed by addition of 5,5'-dithiobis-(2-nitrobenzoic acid) (DTNB) to a concentration of 1 mM and incubation for 10 minutes at 20°C; (3) buffer-exchange into DTT- and DTNB-free crosslinking buffer. In this reaction, DTNB forms a

mixed cysteine-TNB disulfide, with TNB forming an efficient leaving group that promotes disulfide formation in the presence of a second cysteine (Yang *et al*, 2015; Winther & Thorpe, 2014). TRIP13^{W221C} and TRIP13$^{\Delta Cys}$ were mixed in a 1:8 molar ratio in the presence of 1 mM ATP and 5 mM DTT in crosslinking buffer, incubated 60 minutes at 20°C, followed by buffer-exchange to DTT-free crosslinking buffer. p31^{comet} was prepared by incubation in crosslinking buffer + 5 mM DTT for 60 minutes at 20°C, followed by buffer-exchange to DTT-free crosslinking buffer. TRIP13 (20 μM monomers), MAD2 (5 μM), and p31^{comet} (5 μM) were mixed in the presence of 1 mM ATP or ATP-γS for 1 minute at 37°C in crosslinking buffer, then quenching buffer (200 mM iodoacetic acid (IAA), 400 mM Tris-HCl pH 8.5, 6.2 M urea, 2 mM EDTA) was added and samples were analyzed by non-reducing PAGE and Western blotting with anti-MAD2 (Bethyl #A300-301A, 1:5000 dilution) and anti-TRIP13 (Bethyl #A303-605A, 1:5000 dilution) antibodies. For the experiments in **Fig 3C-D** and **Appendix Fig S3D**, the membrane was blotted first for TRIP13, then stripped and blotted for MAD2.

Ion-exchange chromatography and MAD2 conversion assays

For examination of MAD2 conformation, ion-exchange chromatography was carried out largely as described (Ye *et al*, 2015). Briefly, purified proteins or cell extracts (see below) were injected onto a 1 mL Mono-Q column (GE Health Sciences) in buffer containing 50 mM NaCl, then eluted with a gradient to 400 mM NaCl. Fractions were collected, analyzed by SDS-PAGE and visualized by Coomassie staining (purified proteins) or western blot (cell extracts).

For MAD2 conversion assays, 166 μL reactions with separately-purified *M. musculus* MAD2 R133A (full-length or ΔN mutants), p31^{comet}, and TRIP13 were incubated at 20°C for two hours at 30 μM concentration (six-fold molar excess of p31^{comet} and MAD2 to TRIP13 hexamers), in ATPase assay buffer (pH 7.5) with 2 mM ATP. NaCl concentration was diluted to 50 mM, then reactions were analyzed by ion-exchange chromatography as above.

Time-lapse imaging

For cell lines stably expressing siRNA-resistant MAD2 constructs, full-length or N-terminally truncated MAD2 was cloned from cDNA into pCDNA5/FRT/TO (Invitrogen) using a Gibson assembly kit (New England Biolabs). These were incorporated into parental Flp–In TRex–DLD-1 parental cells that stably express mRFP-tagged histone H2B (H2B–mRFP) (Han *et al*, 2013; Holland *et al*, 2010) using FRT/Flp-mediated recombination (Tighe *et al*, 2004). Expression of MAD2 variants were induced with with 1 μg/mL doxycycline. siRNAs directed against the 3' untranslated region of Mad2 (5'-CCUAUUGAAUCAGUUUCCAAUUU-3'; 5'-CAGUAUAGGUAGGGAGAUAUU-3') or GAPDH (5'-UGGUUUACAUGAUCC-AAUA-3') were purchased from GE Dharmacon.

To determine unperturbed mitotic timing, cells were seeded onto CELLSTAR μClear 96-well plate (Greiner bio-one) with 50 nM of oligonucleotides using Lipofectamine RNAiMAX (Thermo Fisher). 24 hr after transfection, doxycline was added to express MAD2 for 24 hr before analyzing by time-lapse microscopy. Cells were maintained at 37°C and 5% CO_2 and images were collected using a CQ1 confocal image cytometer (Yokogawa) with a 40x objective at 10-min time intervals. Movies were assembled and analyzed using ImageJ (National Institutes of Health) software. To measure mitotic slippage, nocodazole was added 1hr before filming.

Mouse spermatocyte protein localization

To overexpress tagged proteins in spermatocytes, we injected 6–8 µl of an expression vector (5 µg/µl) under the control of a CMV promoter into the rete testis of live juvenile CD1 mice (13dpp) according to published protocol (Shibuya *et al*, 2014; Shoji *et al*, 2005). One hour after injection, testes were held between tweezer type of electrodes (CUY650P5, Nepagene) and in vivo electroporation was carried out with four 50-ms pulses (35 Volts) with 950 ms intervals, then four equivalent pulses with opposite polarity (NEPA21 Electroporator, Nepagene). Spermatocytes were collected 24 h after electroporation for the detection of eGFP or 3xFLAG tagged genes in spermatocytes. All animals were used and maintained in accordance with the German Animal Welfare legislation ('Tierschutzgesetz'). All procedures pertaining to animal experiments were approved by the Governmental IACUC ('Landesdirektion Sachsen') and overseen by the animal ethics committee of the Technische Universität Dresden (license number DD24-5131/207/18).

Preparation of nuclear surface spreads of spermatocytes were carried out as described previously (Peters *et al*, 1997). Briefly, testes tubuli were minced in a drop of PBS and resulting suspension was passed through 20 µm filter to remove clumps (Filcon, Cat No:340595). Cell suspensions were diluted 1:2-1:5 with 100 mM sucrose, and 30 µl of diluted cell suspensions were added to microscopic slides covered with 100-120 µl of filtered (0.2 µm) 1% paraformaldehyde (PFA), 0.15% Triton X-100, 1 mM sodium borate pH 9.2 solution and incubated for 80 min at room temperature. Slides were dried at least 1 hour in a fume hood, then washed twice with 0.4% Photoflo (Kodak), once with water, then dried at room temperature. For immunostaining, slides were blocked with 2% BSA, 0.1 % Tween 20, 20 mM sodium azide in PBS for 30 minutes, and then incubated with primary antibodies for 3 hours at room temperature. Slides were then washed 3 x 5 minutes with PBS and incubated with secondary antibodies for 1 hour, then washed 3 x 5 minutes with PBS and mounted in Prolong Diamond AntiFade mountant (ThermoFisher). Primary antibodies used were monoclonal mouse anti-SYCP3 II52F10 (1:1, a gift from R. Jessberger), chicken anti-SYCP3 (1:300, homemade), rabbit anti-SYCP1 (1:1000, Abcam #15090), chicken anti-SYCP1 (1:300, homemade), rabbit anti-GFP (1:1000, ThermoFisher #A11122), monoclonal mouse ANTI-FLAG M2 (1:1000, Sigma-Aldrich #F1804). Goat secondary antibodies conjugated with Alexa Fluor 405 (ThermoFisher #A31553A31556, Abcam #175565), Alexa Fluor 488 (ThermoFisher #A11029/A11034), and Alexa Fluor 568 (ThermoFisher #A11031/11036) were used at 1:600 dilution. Images were acquired with Zeiss Axiophot fluorescence microscope and Axiocam MRm camera, using Axiovision software.

Advanced Photon Source support statement

Portions of this work were conducted at the Northeastern Collaborative Access Team beamlines at the Advanced Photon Source at Argonne National Laboratory, which are funded by the National Institute of General Medical Sciences from the National Institutes of Health (P41 GM103403). The Pilatus 6M detector on 24-ID-C beam line is funded by a NIH-ORIP HEI grant (S10 RR029205). This research used resources of the Advanced Photon Source, a U.S. Department of Energy (DOE) Office of Science User Facility operated for the DOE Office of Science by Argonne National Laboratory under Contract No. DE-AC02-06CH11357.

Data Availability

The crystal structures reported here are available at the Protein Data Bank (http://www.pdb.org) under the accession codes 5VQ9 (TRIP13^{E253Q} Apo; DOI 10.2210/pdb5vq9/pdb) and 5VQA (TRIP13^{E253Q}·ATP; DOI 10.2210/pdb5vqa/pdb). Diffraction datasets for both structures are available at

the SBGrid Data Bank (https://data.sbgrid.org) under the accession codes 409 ($TRIP13^{E253Q}$ Apo; DOI 10.15785/SBGRID/409) and 410 ($TRIP13^{E253Q}$·ATP; DOI 10.15785/SBGRID/410).

Previously-reported crystal structures used here for data interpretation and analysis include those of *C. elegans* PCH2 (PDB ID 4XGU; DOI 10.2210/pdb4xgu/pdb), human MAD2:$p31^{comet}$ complex (PDB ID 2QYF; DOI 10.2210/pdb2qyf/pdb), human MAD2 (PDB ID 2V64; DOI 10.2210/pdb2v64/pdb), and *C. elegans* HTP-1:HIM-3 closure motif complex (PDB ID 4TZO; DOI 10.2210/pdb4tzo/pdb).

Appendix References

Adams PD, Afonine PV, Bunkóczi G, Chen VB, Davis IW, Echols N, Headd JJ, Hung LW, Kapral GJ, Grosse-Kunstleve RW, McCoy AJ, Moriarty NW, Oeffner R, Read RJ, Richardson DC, Richardson JS, Terwilliger TC & Zwart PH (2010) PHENIX: a comprehensive Python-based system for macromolecular structure solution. *Acta Crystallogr D Biol Crystallogr* **66:** 213–221

Andersen KR, Leksa NC & Schwartz TU (2013) Optimized E. coli expression strain LOBSTR eliminates common contaminants from His-tag purification. *Proteins* **81:** 1857–1861

Butt TR, Edavettal SC, Hall JP & Mattern MR (2005) SUMO fusion technology for difficult-to-express proteins. *Protein Expr Purif* **43:** 1–9

Emsley P, Lohkamp B, Scott WG & Cowtan K (2010) Features and development of Coot. *Acta Crystallogr D Biol Crystallogr* **66:** 486–501

Evans PR & Murshudov GN (2013) How good are my data and what is the resolution? *Acta Crystallogr D Biol Crystallogr* **69:** 1204–1214

Han JS, Holland AJ, Fachinetti D, Kulukian A, Cetin B & Cleveland DW (2013) Catalytic assembly of the mitotic checkpoint inhibitor BubR1-Cdc20 by a Mad2-induced functional switch in Cdc20. *Mol Cell* **51:** 92–104

Herzog F, Kahraman A, Boehringer D, Mak R, Bracher A, Walzthoeni T, Leitner A, Beck M, Hartl F-U, Ban N, Malmström L & Aebersold R (2012) Structural probing of a protein phosphatase 2A network by chemical cross-linking and mass spectrometry. *Science* **337:** 1348–1352

Holland AJ, Lan W, Niessen S, Hoover H & Cleveland DW (2010) Polo-like kinase 4 kinase activity limits centrosome overduplication by autoregulating its own stability. *J Cell Biol* **188:** 191–198

Kabsch W (2010) XDS. *Acta Crystallogr D Biol Crystallogr* **66:** 125–132

Kapust RB, Tözsér J, Fox JD, Anderson DE, Cherry S, Copeland TD & Waugh DS (2001) Tobacco etch virus protease: mechanism of autolysis and rational design of stable mutants with wild-type catalytic proficiency. *Protein Eng.* **14:** 993–1000

Karplus PA & Diederichs K (2012) Linking crystallographic model and data quality. *Science* **336:** 1030–1033

Malakhov MP, Mattern MR, Malakhova OA, Drinker M, Weeks SD & Butt TR (2004) SUMO fusions and SUMO-specific protease for efficient expression and purification of proteins. *J. Struct. Funct. Genomics* **5:** 75–86

McCoy AJ, Grosse-Kunstleve RW, Adams PD, Winn MD, Storoni LC & Read RJ (2007) Phaser crystallographic software. *J Appl Crystallogr* **40:** 658–674

Peters AH, Plug AW, van Vugt MJ & de Boer P (1997) A drying-down technique for the spreading of mammalian meiocytes from the male and female germline. *Chromosome Res* **5:** 66–68

Rinner O, Seebacher J, Walzthoeni T, Mueller LN, Beck M, Schmidt A, Mueller M & Aebersold R (2008) Identification of cross-linked peptides from large sequence databases. *Nat Methods* **5:** 315–318

Shibuya H, Morimoto A & Watanabe Y (2014) The dissection of meiotic chromosome movement in mice

using an in vivo electroporation technique. *PLoS Genet* **10:** e1004821

Shoji M, Chuma S, Yoshida K, Morita T & Nakatsuji N (2005) RNA interference during spermatogenesis in mice. *Dev. Biol.* **282:** 524–534

Sironi L, Melixetian M, Faretta M, Prosperini E, Helin K & Musacchio A (2001) Mad2 binding to Mad1 and Cdc20, rather than oligomerization, is required for the spindle checkpoint. *EMBO J* **20:** 6371–6382

Tighe A, Johnson VL & Taylor SS (2004) Truncating APC mutations have dominant effects on proliferation, spindle checkpoint control, survival and chromosome stability. *J Cell Sci* **117:** 6339–6353

Walzthoeni T, Joachimiak LA, Rosenberger G, Röst HL, Malmström L, Leitner A, Frydman J & Aebersold R (2015) xTract: software for characterizing conformational changes of protein complexes by quantitative cross-linking mass spectrometry. *Nat Methods* **12:** 1185–1190

Winther JR & Thorpe C (2014) Quantification of thiols and disulfides. *Biochim. Biophys. Acta* **1840:** 838–846

Yang B, Stjepanovic G, Shen Q, Martin A & Hurley JH (2015) Vps4 disassembles an ESCRT-III filament by global unfolding and processive translocation. *Nat Struct Mol Biol* **22:** 492–498

Ye Q, Rosenberg SC, Moeller A, Speir JA, Su TY & Corbett KD (2015) TRIP13 is a protein-remodeling AAA+ ATPase that catalyzes MAD2 conformation switching. *Elife* **4:** 213